Distributed Acoustic Sensing Using a Large-Volume Airgun Source and Internet Fiber in an Urban Area

Zhenghong Song[1,2], Xiangfang Zeng[*1,3], Baoshan Wang[2], Jun Yang[4], Xiaobin Li[4], and Herbert F. Wang[5]

Abstract

Seismological methods have been widely used to construct subsurface images in urban areas, for both seismological and engineering purposes. However, it remains a challenge to continuously operate a dense array in cities for high-resolution 4D imaging. In this study, we utilized distributed acoustic sensing (DAS) and a 5.2 km long, L-shaped, telecom, fiber-optic cable to record the wavefield from a highly repeatable airgun source located 7–10 km away. No *P*-wave signal was observed, but the *S*-wave signal emerged clearly on the shot-stacked traces, and the arrivals were consistent with collocated geophone traces. Because the signal quality is significantly affected by cable coupling and local noise, three methods can be employed to improve signal-to-noise ratio: (1) stacking contiguous, colinear channels to increase effective gauge length, (2) connecting multiple fibers within a single conduit and stacking collocated channels, and (3) using engineered fiber. In conclusion, the combination of DAS, using internet fiber and an airgun source with proven efficient signal enhancement methods, can provide frequent snapshots of the near surface across an urban area.

Cite this article as Song, Z., X. Zeng, B. Wang, J. Yang, X. Li, and H. F. Wang (2021). Distributed Acoustic Sensing Using a Large-Volume Airgun Source and Internet Fiber in an Urban Area, *Seismol. Res. Lett.* **XX**, 1–11, doi: 10.1785/0220200274.

Introduction

Many highly populated cities face significant seismic hazards associated with geotechnical conditions in the shallow subsurface. For example, many structural collapses causing casualties have been related to subway construction or leaking pipelines. Just as seismological methods have been used to monitor bridge and building health (e.g., Jian *et al.*, 2020), time-lapse seismic tomography could be used to detect velocity changes at shallow depth, to provide early warning for street collapse and other accidents related to sinkholes (e.g., Tran *et al.*, 2013). However, the sizes of velocity anomalies related to sinkholes or velocity changes related to leaking pipelines are relatively small, and high-resolution seismic images are needed to detect such small features. High-resolution shallow structure imaging can be used for microzonation mapping and ground-motion simulation (e.g., Bonnefoy-Claudet *et al.*, 2006) and can monitor changes. Dense arrays with short-period nodal seismometers have been widely used to obtain high-resolution seismic structures beneath cities (e.g., Nakata *et al.*, 2015; Li *et al.*, 2016). However, most nodal seismometers are designed for temporary acquisition. Distributed acoustic sensing (DAS) technology uses relatively permanent fiber-optic cable as the sensing element and provides dense spatial sampling of the wavefield (Parker *et al.*, 2014; Zhan, 2020). The potential applications of DAS in seismological studies, such as earthquake monitoring and shallow structure imaging, have been demonstrated by several groups in various environments (Castongia *et al.*, 2017; Dou *et al.*, 2017; Zeng, Lancelle, *et al.*, 2017; Zeng, Thurber, *et al.*, 2017; Jousset *et al.*, 2018; Li and Zhan, 2018; Parker *et al.*, 2018; Ajo-Franklin *et al.*, 2019; Lellouch *et al.*, 2019; Lindsey *et al.*, 2019; Sladen *et al.*, 2019; Williams *et al.*, 2019; Yu *et al.*, 2019; Zhu and Stensrud, 2019; Booth *et al.*, 2020; Walter *et al.*, 2020; Wang, Williams, *et al.*, 2020). In an urban area, DAS is easy to incorporate with existing cable (dark fiber) that significantly reduces deployment cost (e.g., Martin *et al.*, 2017; Wang, Williams, *et al.*, 2020) and provides high-resolution shallow structure with ambient noise tomography (e.g., Zeng *et al.*, 2019) or horizontal-to-vertical spectral ratio (HVSR) (e.g., Spica *et al.*, 2020).

Seismic velocity sensitivity to stress, porosity, water level changes, and other factors may indicate possible subsurface instability. Ambient noise can be regarded as a repeating

1. State Key Laboratory of Geodesy and Earth's Dynamics, Innovation Academy for Precision Measurement Science and Technology, Chinese Academy of Sciences, Wuhan, China; 2. School of Earth and Space Sciences, University of Science and Technology of China, Hefei, China; 3. CAS Key Laboratory of Computational Geodynamics, University of Chinese Academy of Sciences, Beijing, China; 4. Earthquake Agency of Yunnan Province, Kunming, China; 5. Department of Geoscience, University of Wisconsin–Madison, Madison, Wisconsin, U.S.A.

*Corresponding author: zengxf@whigg.ac.cn

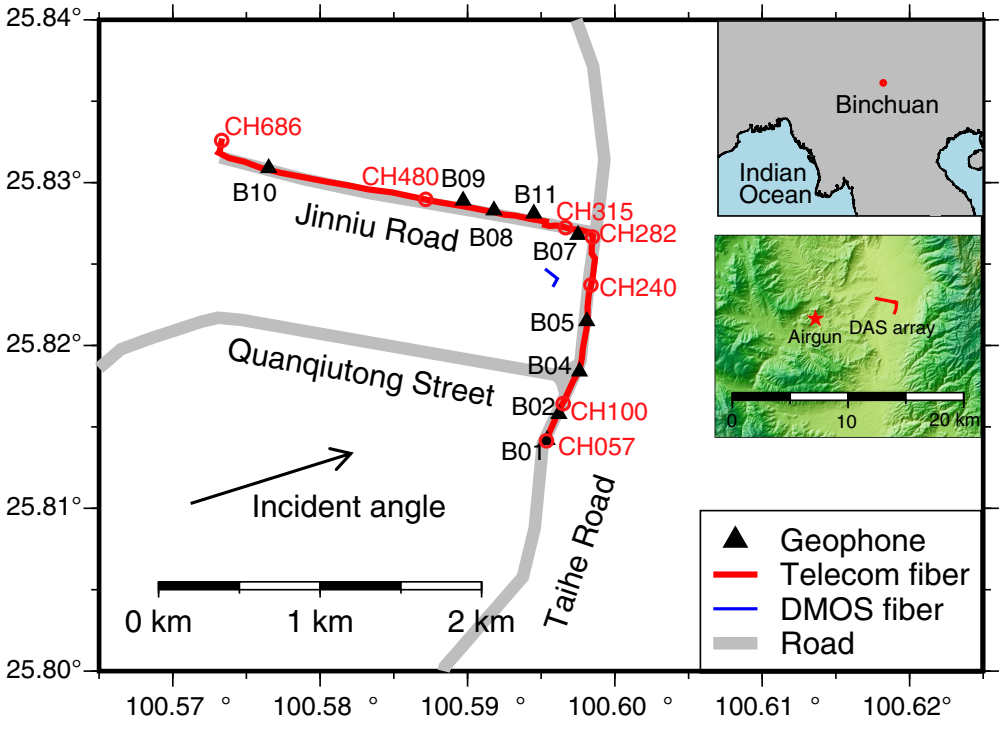

Figure 1. Distributed acoustic sensing (DAS) array (red line) and collocated geophones (triangles). The blue "L" indicates the Distributed Micro-structured Optic Fiber (DMOF) array, and the black arrow is the incident angle. The inset maps show the location of the field site and airgun source. The color version of this figure is available only in the electronic edition.

source, therefore, noise cross-correlation function (NCF) and auto-correlation function (ACF) have been used to study medium changes at various scales (e.g., Xu and Song, 2009; Brenguier *et al.*, 2014; Bennington *et al.*, 2018). Seasonal velocity variation, possibly induced by change in groundwater level, beneath a city was reported from an ambient noise study (Meier *et al.*, 2010) and regionally by Clements and Denolle (2018). However, it takes hours to days to obtain stable NCF or ACF. Another approach is using repeating active sources. This idea can be traced back to the 1960s with dynamite (e.g., Eisler, 1967, 1969). A small airgun source was used to provide a highly repeatable signal, for monitoring in situ stress at levels of earth tides (Reasenberg and Aki, 1974). Because the airgun can be repeatedly shot within a short time period, it is possible to monitor seismic velocity change with high-temporal resolution (Wang, Yang, *et al.*, 2020).

Achieving high-resolution seismic monitoring in a cost-effective way requires selecting system components. Although, DAS provides large spatial coverage at meter-scale resolution, ground coupling is variable, it is natively single component, and it has lower signal-to-noise ratio (SNR) than geophones. The relative lower signal quality also requires efficient noise suppressing method. If ambient noise is the source, long data acquisition times and management of large data sets become an important consideration. In this study, we evaluated a telecom dark-fiber DAS array with a large-volume airgun source, as a practical combination for obtaining sufficiently precise time-dependent changes of seismic properties for urban hazard monitoring.

This article is organized as follows: First, we give an overview of the experimental site, data acquisition, and airgun source. Second, the signal recorded by the DAS array is analyzed with emphasis on stacking repeated airgun shots. Third, we describe additional analysis and fiber-enhancement methodologies to improve signal-to-noise ratio. Finally, we conclude with a discussion of the potential of DAS and internet fiber for subsurface monitoring in urban areas.

Experiment Overview

The experiment was conducted in Binchuan, Yunnan Province, China, in December 2019. Binchuan basin was formed since the Late Cenozoic (Luo *et al.*, 2015). Strong lateral velocity variation at shallow depths have been revealed in previous tomography (Zhang *et al.*, 2020), HVSR (Sun *et al.*, 2019), and seismic wavefield (She *et al.*, 2019) studies. However, a detailed, 3D velocity model in this area is still lacking.

The DAS sensing array consists of 5.2 km of telecom fiber-optic cable lying in 2.5 cm diameter polyvinyl chloride pipe, which was buried at about 30–50 cm depth beneath two streets: Taihe Road and Jinniu Road (Fig. 1). This cable is part of the city of Binchuan's internet distribution network. Each cable typically bundles 132 single-mode fibers in a single jacket. The DAS interrogator configured the cable length into 735 channels with 7.48 m spacing. This channel spacing needs to be distinguished from the 10.9 m gauge length, which represents the spatial resolution. The DAS interrogator records a strain seismogram in continuous mode, with a sampling rate of 500 Hz. For comparisons to be discussed later, nine, short-period three-component geophones were deployed along the cable as well as a short, 150 m, L-shaped array of distributed micro-structured optic fiber (DMOF, e.g., Yu *et al.*, 2018) was installed near the intersection of Taihe and Jinniu Roads between geophones B05 and B07 (Fig. 1).

The source was a large-volume airgun system: fixed airgun signal transmission station (FASTS, Wang, Tian, *et al.*, 2018).

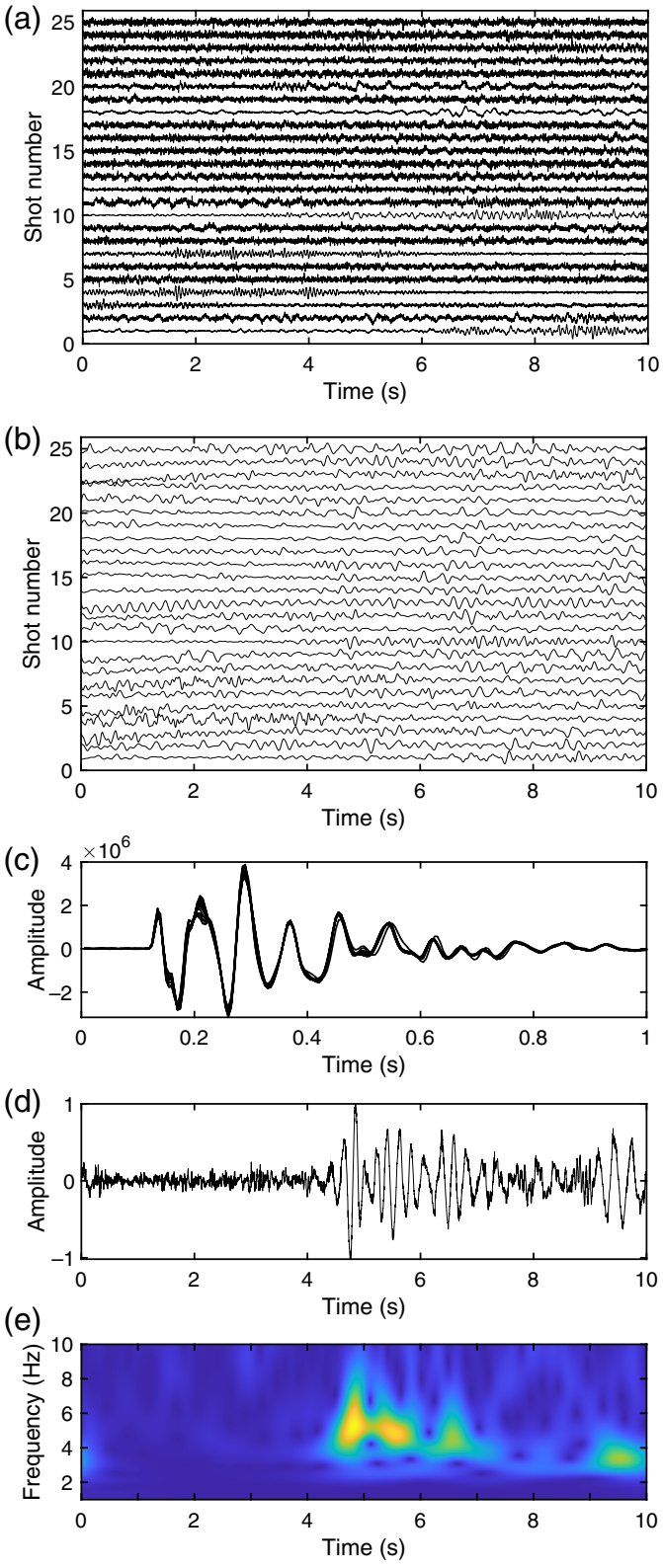

Figure 2. (a) Records of all 25 airgun shots at CH100 during this experiment. (b) The records shown in (a) filtered with a low pass at 10 Hz. (c) 25 traces recorded by a seismometer next to the airgun source. (d) Stacked airgun trace. (e) Time–frequency analysis of the stacked signal. The color version of this figure is available only in the electronic edition.

Source-to-receiver distances ranged between 7 and 10 km. The FASTS is composed of four Bolt LL1500 airguns hanging at about 10 m depth in the Dayindian reservoir. The seismic energy (8.91×10^6 J) released by one shot is equivalent to an M_L 0.7 earthquake. The airgun shots do not disturb nearby aquatic life (Wang *et al.*, 2010) or city residents. The FAST airgun source was developed several years ago, and its repeatability has been analyzed in previous studies in which the cross-correlation coefficient between shots is up to 0.9 (e.g., Wang, Tian, *et al.*, 2018; Li *et al.*, 2020). In our experiment, a reference seismometer next to the source recorded the airgun signal and shows the high repeatability (Fig. 2).

Basic Results

For the Binchuan experiment, the airgun was fired at 15 min intervals from midnight to early morning (local time 00:00–06:00 a.m.), when cultural noise is at a minimum. Figure 2 shows the traces recorded at CH100 for all 25 shots. The individual strain traces are extracted from continuous records and plotted using shot time as the reference time. As shown in Figure 2a, no clear signal is observed on any single trace of CH100. The reason individual traces look very different from each other is because of strong contamination from traffic on Taihe Road above the cable. The traffic noise is temporally random, whereas the airgun signals are coherent. To suppress strong high-frequency ambient noise, the raw waveforms were filtered with a low pass at 10 Hz, and a weak coherent signal emerges around 5 s on filtered waveforms (Fig. 2b). Because the airgun signal is highly repeatable and the noise is random, stacking records from multiple shots can increase the signal quality. We used the time–frequency phase-weighted stacking method (tf-PWS, Schimmel and Gallart, 2007; Zeng and Thurber, 2016), to stack all 25 shot records. One signal emerges on the stacked traces around 4 s after the origin time (Fig. 2d). This arrival time is close to the *S*-wave travel time predicted with a seismic velocity model in this region (Zhang *et al.*, 2020). The SNR, which is defined as the ratio between maximum amplitude of *S*-wave window and root mean square (rms) of amplitude of 2 min of ambient noise before the shot time, increases about 12 times after tf-PWS stacking, whereas the increase is about five times with linear stacking.

Although, the resolution at shallow depth of Zhang's model is limited, the general pattern of the moveout looks reasonable on the record section (Fig. 3). The time–frequency analysis suggests that this signal concentrates in the frequency band from 3 to 8 Hz, which is consistent with the previous study's result (Wang, Tian, *et al.*, 2018).

Every stacked trace across the whole DAS array is band-pass filtered between 3 and 8 Hz and shown in Figure 3. The amplitude varies greatly among channels, which reflects spatial variation of cable coupling, traffic noise level, cable direction, and shallow structure in the basin. As was the case for CH100, the *P*-wave signal is not visible on the most channels. However,

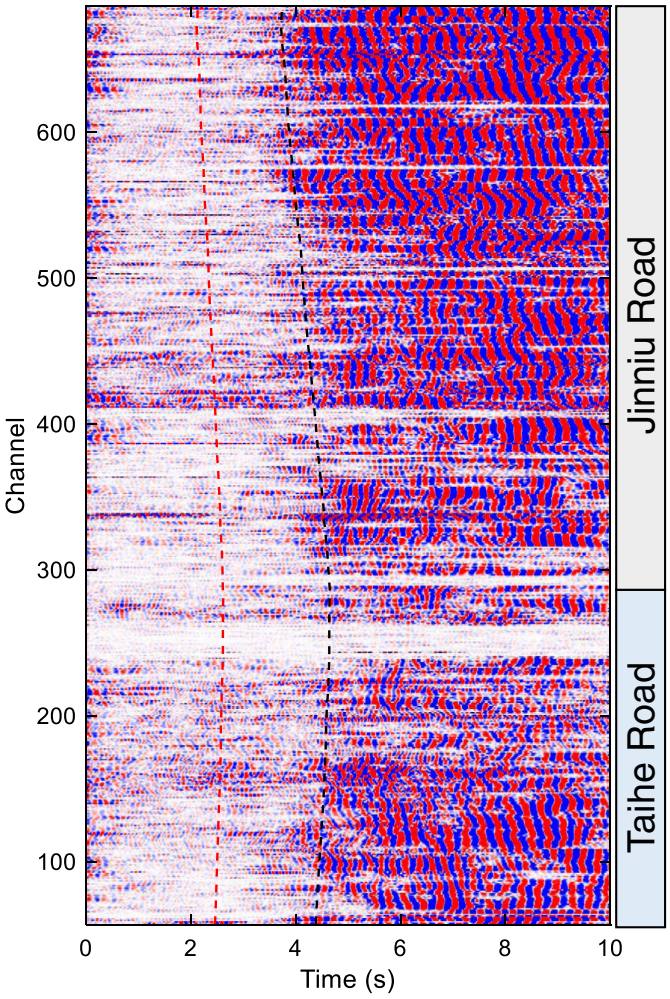

Figure 3. Stacked traces of the whole DAS array. The red and black dashed lines represent theoretical *P*- and *S*-wave arrival times, respectively. All traces have been band-pass filtered between 3 and 8 Hz. The color version of this figure is available only in the electronic edition.

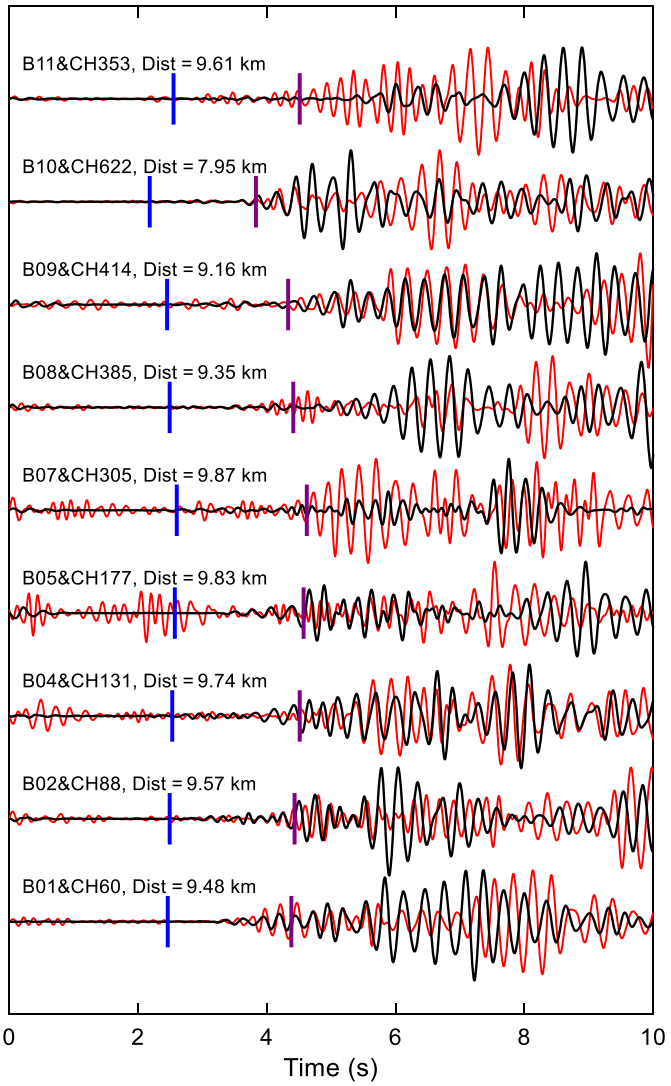

Figure 4. Filtered (between 3 and 8 Hz) and stacked traces of DAS (red lines) and collocated geophones (black lines). The theoretical arrival times of *P* and *S* wave are marked by blue and purple bars, respectively. The theoretical travel times are computed with velocity model developed by Zhang *et al.* (2020). The color version of this figure is available only in the electronic edition.

as with CH100, signals emerge around the theoretical *S*-wave arrival times.

To compare with DAS records, the horizontal components of nine collocated geophones are rotated into the direction of the fiber-optic cable and stacked with the same method. The stacked traces are filtered by a 3–8 Hz band-pass filter (Fig. 4). The theoretical arrival times of *P* and *S* waves are marked by blue and purple bars, respectively. No clear signal is observed around the *P*-wave's arrival time on both geophone and DAS records. The absence of a *P*-wave signal on the horizontal record indicates a steep angle of incidence. On the other hand, signals around the *S*-wave's arrival times are visible on the most records. Therefore, we infer that the signals around 4 s are *S* wave or a related phase.

To investigate the effects of cable coupling and traffic noise, we analyzed the waveforms for 2 min, before each airgun shot. The power spectral density (PSD) of every channel's record is shown in Figure 5a, whereas Figure 5b compares root mean square (rms) noise for 2 s before a shot and maximum signal amplitude between 0 and 10 s after an airgun shot. The record for each channel was first band-pass filtered (3–8 Hz). The frequency range of most noise falls into the typical traffic noise frequency band (5–25 Hz). The heavy truck traffic on Taihe Road induces significantly stronger noise, whereas, most channels along Jinniu Road are much quieter, except channels (CH410-450) around a crossing. Because the amplitude of the tf-PWS stacked traces reflects the coherency, strong random noise that reduces coherence among traces results in weaker signals. The noise level of channels along Taihe Road is obviously

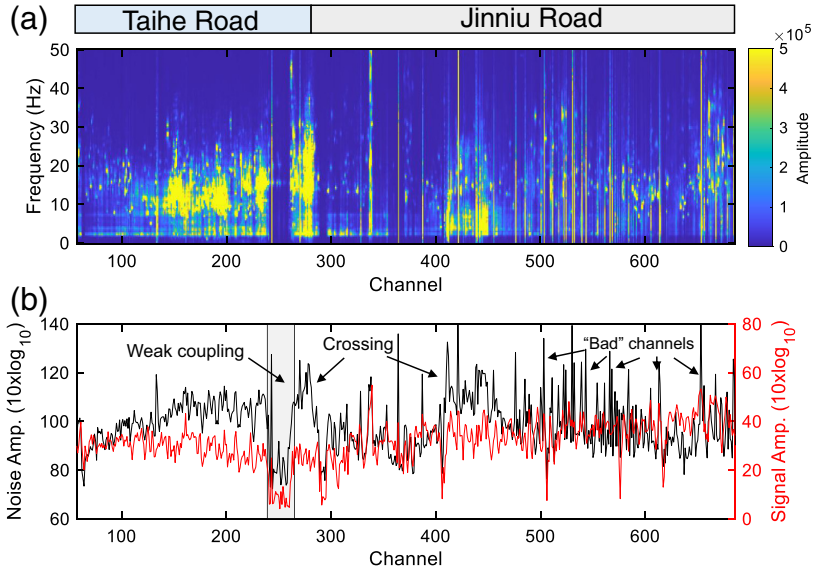

Figure 5. (a) Spectra of ambient noise records. (b) Comparison for every channel of root mean square (rms) amplitude of ambient noise for 2 s before the shot (black) and maximum amplitude of airgun signal between 0 and 10 s after the shot (red). The record from each channel was first band-pass filtered between 3 and 8 Hz. The amplitude is proportional to strain. The color version of this figure is available only in the electronic edition.

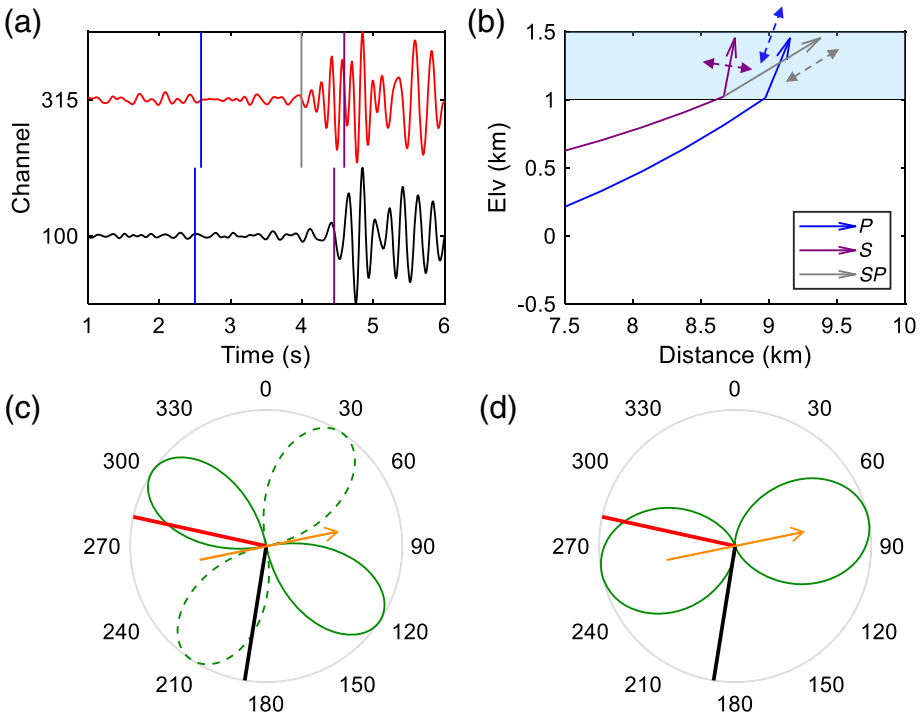

Figure 6. (a) The stacked traces of two representative channels along Taihe Road (CH100, black) and Jinniu Road (CH315, red). The blue and purple bars denote the theoretical arrival times of *P* and *S* waves, respectively, and the gray bar marks the converted phase *SP*. (b) The ray paths and particle motion directions of *P* (blue), *S* (purple), and *SP* (gray). (c,d) DAS strain directional sensitivities of *S* and *P* waves, respectively, in map view. The orange arrow denotes the incident angle in Figure 1, and the green solid and dashed lines mean positive and negative strain, respectively. The red and black lines correspond to the directions of Taihe Road and Jinniu Road, respectively. The color version of this figure is available only in the electronic edition.

higher than those along Jinniu Road (Fig. 5a), and it is expected that airgun signals on channels with stronger ambient noise are weaker (Fig. 5b).There is a clear trough between channels 240–260, and the airgun signal is also weak (Fig. 5b). Hence, we infer that this segment is weakly coupled to the medium (e.g., suspended in a maintenance hole), which was confirmed during the tap test. Several bright streaks are also observed on the PSD figure, which could be due to "bad" channels in which the backscattered optical signal produced a strong artificial strain signal.

Besides the cable coupling and traffic noise, direction changes also affect the signal quality. As a single horizontal component sensor, the directional sensitivity of DAS has been investigated in previous studies (e.g., Bakku, 2015). Figure 6a shows two representative stacked traces (CH100 and CH315) along Taihe Road and Jinniu Road. The signals around 4 s are different on the two channels. On CH100, the arrival time is consistent with the theoretical travel time, which implies that this signal is *S* wave. By contrast, on CH315, the signal arrives about 0.6 s before the theoretical travel time. In the Binchuan basin, a loose sediment layer is revealed by the HVSR method in the top 500 m (Sun *et al.*, 2019). The incident *S* wave may convert into *P* wave (*SP*, Fig. 6b) at the bottom of the sediment. The particle motion of *SP* suggests that the amplitude of *SP* on the horizontal component is stronger than the *P* wave. The travel-time difference between *SP* and *S* depends on the V_P/V_S ratio and thickness of sediment.

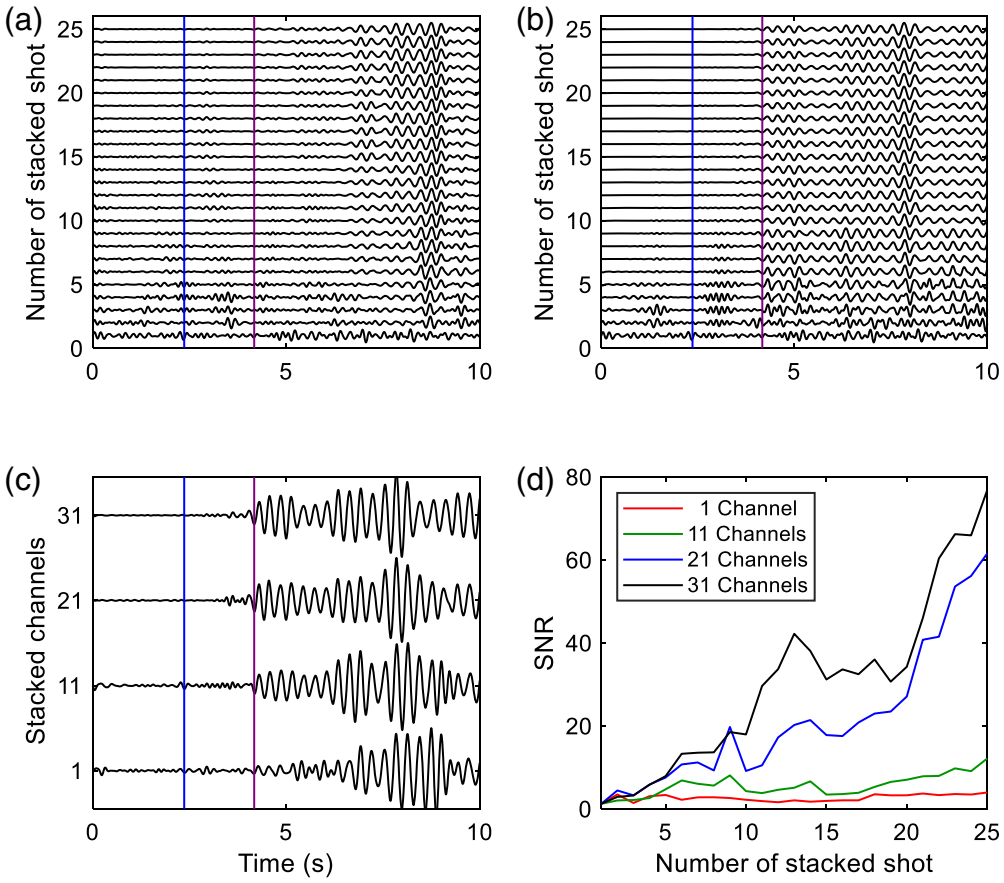

Figure 7. Shot-stacked traces for different effective gauge lengths. The blue and dark purple lines in (a)–(c) are the expected *P*- and *S*-wave arrival times, respectively. (a) Stacked traces of 1 channel (10 m effective gauge length). (b) Stacked traces of 31 channels (225 m effective gauge length). (c) Stacked traces of four effective gauge lengths ranging from one channel to 31 channels. (d) The signal-to-noise ratio (SNR) convergence curves for different gauge lengths. The color version of this figure is available only in the electronic edition.

According to the previous study, the sediment is about 500 m thick, and the average *S*-wave speed is about 500 m/s (Sun *et al.*, 2019). Using a typical V_P/V_S ratio (4.0) in sediment (Bao *et al.*, 2019), the travel-time difference between *S* and *SP* is about 0.75 s, which is close to our observation. Therefore, we infer that the wave train around 4 s on the CH315 is composed of both *SP* and *S*-wave signals. The absence of *SP* on CH100 can be explained in terms of directional response. As shown in Figure 6c,d, the channels along Jinniu Road are expected to show a stronger response for both *P* and *S* waves.

Methods to Enhance Signal-to-Noise Ratio

As described earlier, it is feasible to use telecom fiber-optic cable in an urban area, to record the seismic wavefield excited by a large-volume airgun system. In this section, we discuss three methods to improve SNR that can be implemented in DAS telecom arrays. In order of simplicity, they are (1) stacking a greater number of channels, to increase effective gauge length, (2) connecting multiple fibers within a single conduit and stacking collocated channels, and (3) using engineered fibers. Implementation of these methods could allow using lower energy repeatable sources, for example, continuous active source seismic monitoring (CASSM) (Ajo-Franklin *et al.*, 2011) or suborbital vibrators (SOVs) (e.g., Dou *et al.*, 2016).

Channel stacking to increase effective gauge length

As discussed in previous studies, DAS records strain integrated or averaged over the gauge length. The gauge length plays an important role in signal quality (Dean *et al.*, 2016). The gauge length in an interrogator is either set up by the manufacturer or chosen by the user before acquisition. After acquisition, linearly stacking a group of channels effectively increases gauge length (Wang, Zeng, *et al.*, 2018). Dean *et al.* (2016) suggested that the optimal gauge length is about 0.6 times wavelength, which is a function of apparent velocity and frequency. In this experiment, the wavelength of the *S* wave is about 400 m. Summing over traces of a group of channels, centered at CH480 from a single shot, is effectively simulating longer gauge lengths. The tf-PWS stacked traces of all 25 shots for a single channel (10.9 m effective gauge length) (Fig. 7a) are compared with averaging over 31 channels (225 m effective gauge length) (Fig. 7b). The *S*-wave arrival appears after stacking five shots using the longer effective gauge length, whereas it remains in the noise even after stacking 25 shots using the interrogator's built-in gauge length. However, in Figure 7b, stacking more shots is still needed to suppress local traffic noise. Figure 7c shows how increasing effective gauge length by stacking 11, 21, and 31 channels, whereas also stacking all 25 shots, brings out the *S*-wave arrival clearly with 11 channels (75 m effective gauge length). SNR curves for different effective gauge lengths, as a function of number of shots stacked (Fig. 7d), confirm that longer effective gauge lengths also improve SNR, which reduces either the number of shots or energy of each shot needed to obtain reliable records. Here, the SNR is computed as the maximum amplitude

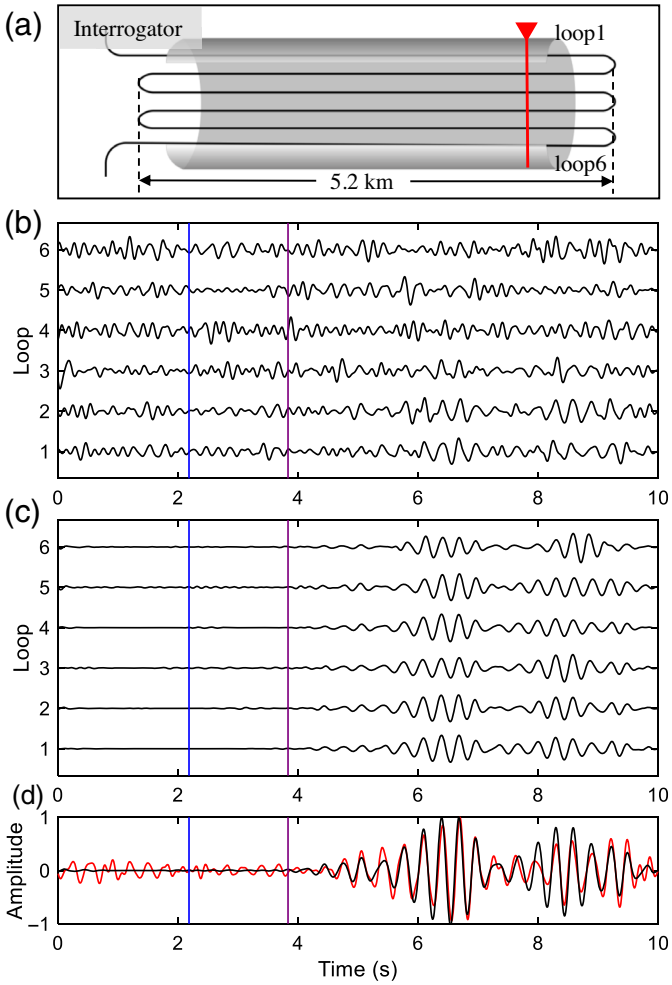

Figure 8. (a) Sketch of the multiple optical fibers in a single cable. (b) Records of individual collocated channels (red line in a) in a single cable of a single shot. (c) Record of individual traces after stacking 25 shots. (d) Record of stacked traces of six channels of a single shot (red) versus 25-shot stack of one channel. The theoretical arrivals of *P* and *S* waves are marked by blue and purple lines, respectively. The color version of this figure is available only in the electronic edition.

in the signal window (±0.5 s around theoretical *S*-wave arrival) over the rms amplitude of the noise window (0–0.5 s before theoretical *P*-wave arrival). However, increasing gauge length only works well when assumptions of uniform coupling, homogenous structure, and constant incident angle are met.

Stacking multiple, collocated fibers within cable

Another solution that is not affected by the spatial variation of coupling and shallow structure is sampling a single location by multiple fibers in one cable. Tens of optical fibers are assembled in one telecom cable, and several can be spliced together (Fig. 8a). Both—the random optical noise and ambient seismic noise strongly—affect the waveforms (Fig. 5b), and one shot of the airgun signal is too weak to be observed on a single channel's record (Fig. 8b). As previously discussed, coherent waveforms are obtained via stacking 25 shots (Fig. 8c). But, also stacking six collocated channels from a single shot results in a reasonable waveform, and the signal quality is comparable to stacking traces of 25 shots (Fig. 8d). Because this strategy improves signal quality without losing in spatial resolution, it will be useful in small aperture DAS arrays. The method involves investment in splicing multiple fibers and requires cooperation of telecom providers. Additional storage and computational cost are also required and will benefit from newly developed parallel storage and analysis frameworks (e.g., Dong *et al.*, 2020).

Using engineered cable

Besides standard telecom fiber-optic cable, engineered fiber-optic cable has also been introduced to improve DAS sensitivity (e.g., Kuvshinov, 2016; Yu *et al.*, 2018). A 150 m DMOF cable was deployed in an "L"-shaped trench in Binchuan (blue "L" in Fig. 1). A series of ultraweak FiberBragg Gratings were built in the DMOF optical fiber, every 2 m. The grating reflects the incident laser pulse much more strongly than Rayleigh backscatter from random scatterers and is, therefore, much more sensitive to the dynamic strain of the seismic wavefield. In addition, the trench was backfilled with wet sand that provided much better coupling than was the case for telecom cable. The airgun signal could be identified from a single shot (Fig. 9a). Traffic signals were visible when only a few shots were stacked. The traffic signal was removed after about five shots in much the same way as a long photographic exposure removes people from a scene. Comparing to a nearby channel on the telecom cable, the SNR of trenched-DMOF data increased much more rapidly, with the number of stacked shots. A more diagnostic test of the relative advantage of DMOF would require a comparison in which it was bundled with regular telecom fiber.

Discussion

Deploying and maintaining a dense seismic array in an urban area is a big challenge using a network of classic seismometers and geophones (Cochran, 2018). Alternatives, such as new, low-cost Micro Electro Mechanical Systems sensors deployed in a smartphone Internet of Things environment (e.g., Quake-Catcher-Network; Cochran *et al.*, 2009), MyShake (Rochford *et al.*, 2018) or in an all-in-one device (e.g., Raspberry Shaken (Anthony *et al.*, 2019) have been introduced in the past decade primarily for earthquake detection, where the hazard is high. However, such low-cost sensors still have difficulties in accurate timing and real-time data transfer. Because a DAS interrogator acquires data from the whole array at a single instant in time, array and real-time data processing are possible.

Monitoring as a function of time is required to detect subsurface medium change. Besides the airgun source used in this study, various environment-friendly repeatable active sources have been used in different frequency bands. The high-frequency piezoelectric source CASSM (Ajo-Franklin *et al.*,

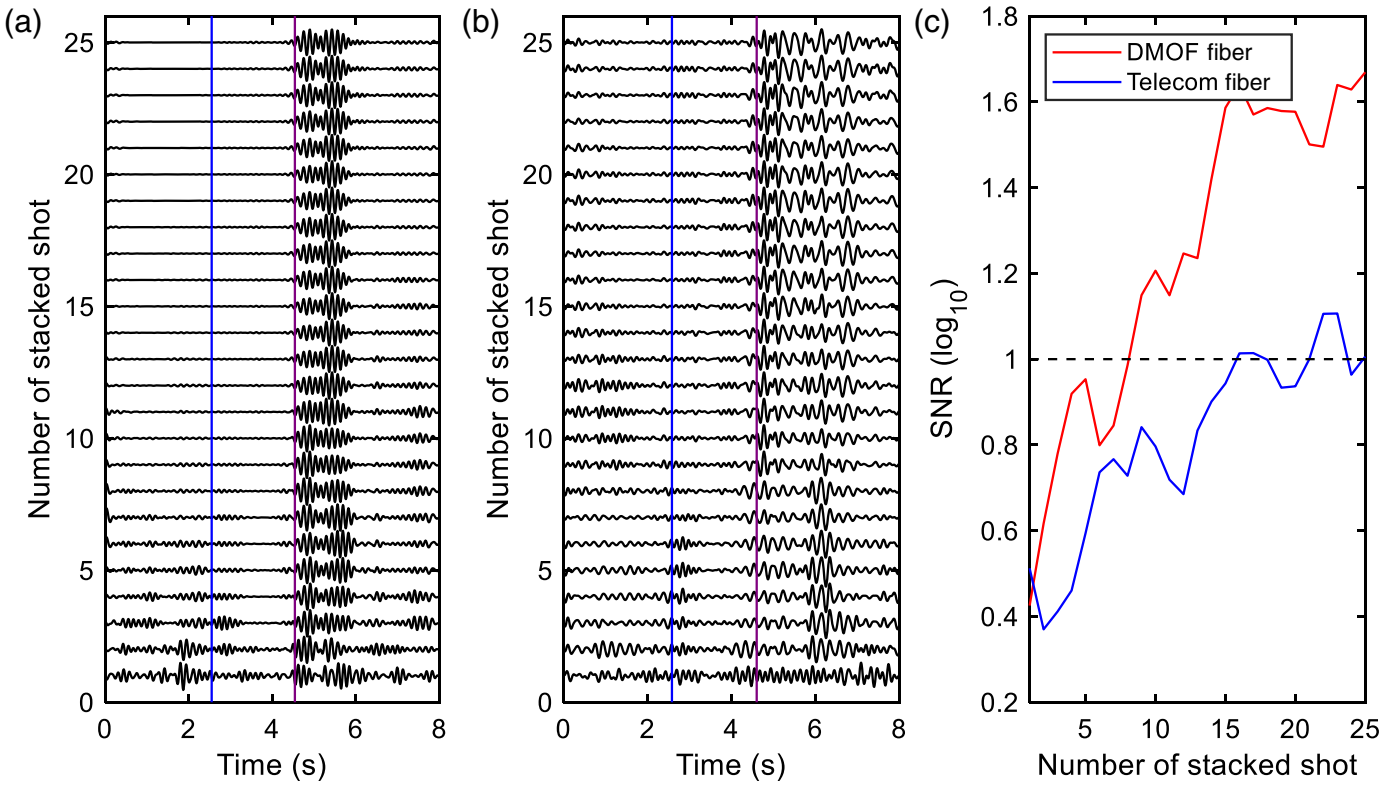

Figure 9. (a) Stacked traces of one DMOF channel. (b) Stacked traces of one nearby telecom cable channel. (c) The SNR curves of two types of standard versus engineered fiber-optic cable. The color version of this figure is available only in the electronic edition.

2011) was used to monitor velocity change due to fracturing. A similar source was also used in San Andreas Fault Observatory at Depth to study velocity changes around two earthquakes at Parkfield, California (Niu *et al.*, 2008). A small SOV device was introduced to monitor a CO_2 storage site in Australia (e.g., Dou *et al.*, 2016). The Accurately Controlled Routinely Operated Signal System source was also used to monitor a CO_2 storage site in Canada (Ikeda *et al.*, 2017). These highly repeatable sources can be deployed on spatial grids in urban area, to increase ray coverage. Besides active sources, a seismic signal emerging from NCFs also has a potential to track groundwater (e.g., Clements and Denolle, 2018). Combining repeatable sources with telecom cable in an urban area makes it possible to detect small velocity changes due to construction (e.g., Fang *et al.*, 2020), groundwater level change, and so forth.

As described in our Binchuan experiment, the signal from a single shot is much weaker than the background noise. Both engineered cable and multiple fibers bundled within single cable can be deployed in high-risk or high-population areas, to improve the SNR significantly. Local seismic noise can be suppressed by stacking nearby channels. Time–frequency phase-weighted stacking is highly effective for signal extraction, and, thereby, improve temporal resolution.

Conclusions

A 5.2 km long, existing telecom fiber-optic cable in Binchuan (population 330,000), a small city in China, was used as a dense seismic array with the novel DAS technology. The DAS array recorded the seismic wavefield excited by repeated shots from a large-volume airgun, and the records are consistent with collocated geophone data. The signal quality reflects the spatial variation of cable coupling and background traffic noise. The *P*-wave signal is absent on most channels, because of its almost vertical incidence and weak broadside directional sensitivity of horizontally oriented cable. The *S* wave converted to *P* wave, at the bottom of sediment (*SP*), arrives earlier than the *S* wave on part of the array. Three methods can improve signal quality: (1) increasing the number of traces stacked spatially, which effectively increases gauge length, (2) sampling one location with multiple fiber connected within a single cable, and (3) using engineered optical fiber. In summary, it is feasible to combine a DAS array and a highly repeatable airgun source into a high-resolution subsurface medium monitoring system.

Data and Resources

Data used in this study are available upon request to the corresponding author Xiangfang Zeng.

Acknowledgments

The authors thank China Mobile Binchuan Company for providing access to telecom cable and assistance in the field. Fotech Group

Limited provided a Helios Theta distributed acoustic sensing (DAS) interrogator for the internet fiber cable data acquisition. The authors also thank Clifford Thurber (University of Wisconsin, Madison), Yunpeng Zhang (China Earthquake Administration), and Weitao Wang (China Earthquake Administration) for their constructive comments and suggestions. This article also benefitted from comments from two anonymous reviewers and editors. This work was supported by the National Natural Science Foundation of China under Grant Numbers 41974067, 41790462 and Chen Yong Academician Workstation of Yunnan Province in China (2014IC007).

References

Ajo-Franklin, J., T. Daley, B. Butler-Veytia, J. Peterson, Y. Wu, B. Kelly, and S. Hubbard (2011). Multi-level continuous active source seismic monitoring (ML-CASSM): Mapping shallow hydrofracture evolution at a TCE contaminated site, *SEG Technical Program Expanded Abstracts 2011*, Society of Exploration Geophysicists, 3727–3731.

Ajo-Franklin, J. B., S. Dou, N. J. Lindsey, I. Monga, C. Tracy, M. Robertson, V. R. Tribaldos, C. Ulrich, B. Freifeld, T. Daley, *et al.* (2019). Distributed acoustic sensing using dark fiber for near-surface characterization and broadband seismic event detection, *Sci. Rep.* **9,** no. 1, 1–14.

Anthony, R. E., A. T. Ringler, D. C. Wilson, and E. Wolin (2019). Do low-cost seismographs perform well enough for your network? An overview of laboratory tests and field observations of the OSOP Raspberry Shake 4D, *Seismol. Res. Lett.* **90,** no. 1, 219–228.

Bakku, S. K. (2015). Fracture characterization from seismic measurements in a borehole, *Ph.D. Thesis*, Massachusetts Institute of Technology, Cambridge, Massachusetts.

Bao, F., Z. Li, B. Tian, L. Wang, and G. Tu (2019). Sediment thickness variations of the Tangshan fault zone in North China from a dense seismic array and microtremor survey, *J. Asian Earth Sci.* **185,** 104045.

Bennington, N., M. Haney, C. Thurber, and X. Zeng (2018). Inferring magma dynamics at Veniamin of volcano via application of ambient noise, *Geophys. Res. Lett.* **45,** no. 21, 11,650–11,658.

Bonnefoy-Claudet, S., F. Cotton, and P. Y. Bard (2006). The nature of noise wavefield and its applications for site effects studies: A literature review, *Earth Sci. Rev.* **79,** nos. 3/4, 205–227.

Booth, A. D., P. Christoffersen, C. Schoonman, A. Clarke, B. Hubbard, R. Law, S. H. Doyle, T. R. Chudley, and A. Chalari (2020). Distributed acoustic sensing of seismic properties in a borehole drilled on a fast-flowing Greenlandic outlet glacier, *Geophys. Res. Lett.* **47,** no. 13, e2020GL088148, doi: 10.1029/2020GL088148.

Brenguier, F., M. Campillo, T. Takeda, Y. Aoki, N. M. Shapiro, X. Briand, K. Emoto, and H. Miyake (2014). Mapping pressurized volcanic fluids from induced crustal seismic velocity drops, *Science* **345,** no. 6192, 80–82.

Castongia, E., H. F. Wang, N. Lord, D. Fratta, M. Mondanos, and A. Chalari (2017). An experimental investigation of distributed acoustic sensing (DAS) on lake ice, *J. Environ. Eng. Geophys.* **22,** no. 2, 167–176.

Clements, T., and M. A. Denolle (2018). Tracking groundwater levels using the ambient seismic field, *Geophys. Res. Lett.* **45,** no. 13, 6459–6465.

Cochran, E. S. (2018). To catch a quake, *Nat. Comm.* **9,** no. 1, 1–4.

Cochran, E. S., J. F. Lawrence, C. Christensen, and R. Jakka (2009). The quake-catcher network: Citizen science expanding seismic horizons, *Seismol. Res. Lett.* **80,** 26–30.

Dean, T., T. Cuny, and A. H. Hartog (2016). The effect of gauge length on axially incident P-waves measured using fibre optic distributed vibration sensing, *Geophys. Prospect.* **65,** no. 1, 184–193.

Dong, B., V. R. Tribaldos, X. Xing, S. Byna, J. Ajo-Franklin, and K. Wu (2020). DASSA: Parallel DAS data storage and analysis for subsurface event detection, *2020 IEEE International Parallel and Distributed Processing Symposium (IPDPS)*, New Orleans, Louisiana, 21 May 2020, IEEE, 254–263.

Dou, S., J. Ajo-Franklin, T. Daley, M. Robertson, T. Wood, B. Freifeld, R. Pevzner, J. Correa, K. Tertyshnikov, M. Urosevic, *et al.* (2016). Surface orbital vibrator (SOV) and fiber-optic DAS: Field demonstration of economical, continuous-land seismic time-lapse monitoring from the Australian CO2CRC Otway site, *SEG Technical Program Expanded Abstracts 2016*, Tulsa, Oklahoma, 22 October 2016, Society of Exploration Geophysicists,5552–5556.

Dou, S., N. Lindsey, A. M. Wagner, T. M. Daley, B. Freifeld, M. Robertson, J. Peterson, C. Ulrich, E. R. Martin, and J. B. Ajo-Franklin (2017). Distributed acoustic sensing for seismic monitoring of the near surface: A traffic-noise interferometry case study, *Sci. Rep.* **7,** no. 1, 1–12.

Eisler, J. D. (1967). Investigation of a method for determining stress accumulation at depth, *Bull. Seismol. Soc. Am.* **57,** no. 5, 891–911.

Eisler, J. D. (1969). Investigation of a method for determining stress accumulation at depth-II, *Bull. Seismol. Soc. Am.* **59,** no. 1, 43–58.

Fang, G., Y. E. Li, Y. Zhao, and E. R. Martin (2020). Urban near-surface seismic monitoring using distributed acoustic sensing, *Geophys. Res. Lett.* **47,** no. 6, e2019GL086115, doi: 10.1029/2019GL086115.

Ikeda, T., T. Tsuji, M. Takanashi, I. Kurosawa, M. Nakatsukasa, A. Kato, K. Worth, D. White, and B. Roberts (2017). Temporal variation of the shallow subsurface at the Aquistore CO2 storage site associated with environmental influences using a continuous and controlled seismic source, *J. Geophys. Res.* **122,** no. 4, 2859–2872.

Jian, J., R. Snieder, and N. Nakata (2020). Extracting the response of the Bay Bridge, California, from the application of multichannel deconvolution to earthquake-induced shaking, *Bull. Seismol. Soc. Am.* **110,** no. 2, 556–564.

Jousset, P., T. Reinsch, T. Ryberg, H. Blanck, A. Clarke, R. Aghayev, G. P. Hersir, J. Henninges, M. Weber, and C. M. Krawczyk (2018). Dynamic strain determination using fibre-optic cables allows imaging of seismological and structural features, *Nat. Comm.* **9,** no. 1, 1–11.

Kuvshinov, B. N. (2016). Interaction of helically wound fibre-optic cables with plane seismic waves, *Geophys. Prospect.* **64,** no. 3, 671–688.

Lellouch, A., S. Yuan, Z. Spica, B. Biondi, and W. L. Ellsworth (2019). Seismic velocity estimation using passive downhole distributed acoustic sensing records: Examples from the San Andreas fault observatory at depth, *J. Geophys. Res.* **124,** no. 7, 6931–6948.

Li, C., H. Yao, H. Fang, X. Huang, K. Wan, H. Zhang, and K. Wang (2016). 3D near surface shear wave velocity structure from ambient noise tomography and borehole data in the Hefei urban area, China, *Seismol. Res. Lett.* **87,** no. 4, 882–892.

Li, X., Z. Song, J. Yang, X. Zeng, and B. Wang (2020). Monitoring signal of airgun source with distributed acoustic sensing, *Seismol. Geol.* **42,** no. 5, doi: 10.3969/j.issn.0253-4967.2020.05.015.

Li, Z., and Z. Zhan (2018). Pushing the limit of earthquake detection with distributed acoustic sensing and template matching: A case study at the Brady geothermal field, *Geophys. J. Int.* **215,** no. 3, 1583–1593.

Lindsey, N. J., T. C. Dawe, and J. B. Ajo-Franklin (2019). Illuminating seafloor faults and ocean dynamics with dark fiber distributed acoustic sensing, *Science* **366,** no. 6469, 1103–1107.

Luo, R. J., Z. H. Wu, X. L. Huang, C. Zhou, and T. Tian (2015). The main active faults and the active tectonic system of Binchuan area, northwestern Yunnan, *Geol. Bull. China* **34,** no. 1, 155–170.

Martin, E. R., C. M. Castillo, S. Cole, P. S. Sawasdee, S. Yuan, R. Clapp, M. Karrenbach, and B. L. Biondi (2017). Seismic monitoring leveraging existing telecom infrastructure at the SDASA: Active, passive, and ambient-noise analysis, *The Leading Edge* **36,** no. 12, 1025–1031.

Meier, U., N. M. Shapiro, and F. Brenguier (2010). Detecting seasonal variations in seismic velocities within Los Angeles basin from correlations of ambient seismic noise, *Geophys. J. Int.* **181,** no. 2, 985–996.

Nakata, N., J. P. Chang, J. F. Lawrence, and P. Boué (2015). Body wave extraction and tomography at Long Beach, California, with ambient-noise interferometry, *J. Geophys. Res.* **120,** no. 2, 1159–1173.

Niu, F., P. G. Silver, T. M. Daley, X. Cheng, and E. L. Majer (2008). Preseismic velocity changes observed from active source monitoring at the Parkfield SAFOD drill site, *Nature* **454,** no. 7201, 204–208.

Parker, L. M., C. H. Thurber, X. Zeng, P. Li, N. E. Lord, D. Fratta, H. F. Wang, M. C. Robertson, A. M. Thomas, M. S. Karplus, *et al.* (2018). Active-source seismic tomography at the Brady Geothermal Field, Nevada, with dense nodal and fiber-optic seismic arrays, *Seismol. Res. Lett.* **89,** no. 5, 1629–1640.

Parker, T. R., S. V. Shatalin, and M. Farhadiroushan (2014). Distributed acoustic sensing-a new tool for seismic applications, *First Break* **32,** no. 2, 61–69.

Reasenberg, P., and K. Aki (1974). A precise, continuous measurement of seismic velocity for monitoring in situ stress, *J. Geophys. Res.* **79,** no. 2, 399–406.

Rochford, K., J. Strauss, Q. Kong, and R. M. Allen (2018). MyShake: Using human-centered design methods to promote engagement in a smartphone-based global seismic network, *Front. Earth Sci.* **6,** 237, doi: 10.3389/feart.2018.00237.

Schimmel, M., and J. Gallart (2007). Frequency-dependent phase coherence for noise suppression in seismic array data, *J. Geophys. Res.* **112,** no. B04303, doi: 10.1029/2006JB004680.

She, Y., H. Yao, W. Wang, and B. Liu (2019). Characteristics of seismic wave propagation in the Binchuan region of Yunnan using a dense seismic array and large volume airgun shots, *Earthq. Res. China* **33,** no. 2, 174–185.

Sladen, A., D. Rivet, J. P. Ampuero, L. De Barros, Y. Hello, G. Calbris, and P. Lamare (2019). Distributed sensing of earthquakes and ocean-solid Earth interactions on seafloor telecom cables, *Nat. Comm.* **10,** no. 1, 1–8.

Spica, Z. J., M. Perton, E. R. Martin, G. C. Beroza, and B. Biondi (2020). Urban seismic site characterization by fiber-optic seismology, *J. Geophys. Res.* **125,** no. 3, e2019JB018656, dio: 10.1029/2019JB018656.

Sun, T., W. Wang, and B. Wang (2019). Using a dense array and HVSR to obtain the shallow structure of the Binchuan Basin, *International Symposium on Deep Earth Exploration and Practices*, Beijing, China, 24–26 October 2018.

Tran, K. T., M. McVay, M. Faraone, and D. Horhota (2013). Sinkhole detection using 2D full seismic waveform tomography, *Geophysics* **78,** no. 5, R175–R183.

Walter, F., D. Gräff, F. Lindner, P. Paitz, M. Köpfli, M. Chmiel, and A. Fichtner (2020). Distributed acoustic sensing of microseismic sources and wave propagation in glaciated terrain, *Nat. Comm.* **11,** no. 1, 1–10.

Wang, B., X. Tian, Y. Zhang, Y. Li, W. Yang, B. Zhang, W. Wang, J. Yang, and X. Li (2018). Seismic signature of an untuned large-volume airgun array fired in a water reservoir, *Seismol. Res. Lett.* **89,** no. 3, 983–991.

Wang, B., W. Yang, W. Wang, J. Yang, X. Li, and B. Ye (2020). Diurnal and semidiurnal P- and S-wave velocity changes measured using an airgun source, *J. Geophys. Res.* **125,** no. 1, doi: 10.1029/2019JB018218.

Wang, B., W. Yang, S. Yuan, S. Guo, H. Ge, P. Xu, and Y. Chen (2010). An experimental study on the excitation of large volume airguns in a small volume body of water, *J. Geophys. Eng.* **7,** 388–394.

Wang, H. F., X. Zeng, D. E. Miller, D. Fratta, K. L. Feigl, C. H. Thurber, and R. J. Mellors (2018). Ground motion response to an ML 4.3 earthquake using co-located distributed acoustic sensing and seismometer arrays, *Geophys. J. Int.* **213,** no. 3, 2020–2036.

Wang, X., E. F. Williams, M. Karrenbach, M. G. Herráez, H. F. Martins, and Z. Zhan (2020). Rose Parade seismology: Signatures of floats and bands on optical fiber, *Seismol. Res. Lett.* **91,** no. 4, 2395–2398.

Williams, E. F., M. R. Fernández-Ruiz, R. Magalhaes, R. Vanthillo, Z. Zhan, M. González-Herráez, and H. F. Martins (2019). Distributed sensing of microseisms and teleseisms with submarine dark fibers, *Nat. Comm.* **10,** no. 1, 1–11.

Xu, Z. J., and X. Song (2009). Temporal changes of surface wave velocity associated with major Sumatra earthquakes from ambient noise correlation, *Proc. Natl. Acad. Sci.* **106,** no. 34, 14,207–14,212.

Yu, C., Z. Zhan, N. J. Lindsey, J. B. Ajo-Franklin, and M. Robertson (2019). The potential of DAS in teleseismic studies: Insights from the Goldstone experiment, *Geophys. Res. Lett.* **46,** no. 3, 1320–1328.

Yu, G., Q. Sun, F. Ai, Z. Yan, H. Li, and F. Li (2018). Micro-structured fiber distributed acoustic sensing system for borehole seismic survey, *SEG Technical Program Expanded Abstracts 2018*, Society of Exploration Geophysicists, 4669–4673.

Zeng, X., and C. H. Thurber (2016). A graphics processing unit implementation for time-frequency phase-weighted stacking, *Seismol. Res. Lett.* **87,** no. 2A, 358–362.

Zeng, X., C. Lancelle, C. Thurber, D. Fratta, H. Wang, N. Lord, A. Chalari, and A. Clarke (2017). Properties of noise cross-correlation functions obtained from a distributed acoustic sensing array at Garner Valley, California, *Bull. Seismol. Soc. Am.* **107,** no. 2, 603–610.

Zeng, X., C. H. Thurber, H. F. Wang, and D. Fratta (2017). 3D shear wave velocity structure revealed with ambient noise tomography on a DAS array, *AGUFM*, 11–15 December 2017, New Orleans, Louisiana, S33F-06.

Zeng, X., B. Wang, X. Li, W. Xu, S. Xu, and Z. Song (2019). Shallow vs structure imaged with the ambient noise recorded by a telecommunication fiber-optic cable in Urban area, *2019 SSA Annual Meeting*, Seattle, Washington, 23–26 April 2019

Zhan, Z. (2020). Distributed acoustic sensing turns fiber-optic cables into sensitive seismic antennas, *Seismol. Res. Lett.* **91,** no. 1, 1–15.

Zhang, Y. P., B. C. Wang, G. C. Lin, W. T. Wang, W. Yang, and Z. H. Wu (2020). Upper crustal velocity structure of Binchuan, Yunnan revealed by dense array local seismic tomography, *Chin. J. Geophys.* **63,** no. 9, 3292–3306.

Zhu, T., and D. J. Stensrud (2019). Characterizing thunder-induced ground motions using fiber-optic distributed acoustic sensing array, *J. Geophys. Res.* **124,** no. 23, 12,810–12,823.

Manuscript received 4 August 2020
Published online 6 January 2021